PERGAMON

International Journal of Heat and Mass Transfer 42 (1999) 249–261

International Journal of HEAT and MASS TRANSFER

Short time-scale radiative transfer in light-emitting porous silicon

M. Cynthia Hipwell*, C. L. Tien

University of California, Berkeley, CA 94720, U.S.A.

Received 20 November 1997; in final form 1 April 1998

Abstract

In this work, a five level system is proposed to model the short time-scale radiative transfer in light-emitting porous silicon. Equations are derived for the various energy levels. The model is applied to picosecond differential transmission measurements made on porous silicon. A picture of short time-scale carrier dynamics is drawn considering the unique properties of confinement, high surface-to-volume ratio and disorder on several length scales.

Nomenclature

A rate for band-to-band absorption [s^{-1}]
A_l laser beam spot area [m^2]
C_p specific heat [J kg^{-1} K^{-1}]
D_{th} diffusion coefficient [m^2 s^{-1}]
E energy [J or eV]
Fo Fourier number [s]
h film thickness [m]
h Planck's constant $= 6.62620 \times 10^{-34}$ J s
I intensity [W m^{-2}]
K_λ spectral absorption coefficient [m^{-1}]
K absorption coefficient [m^{-1}]
k nonradiative recombination rate [s^{-1}]
L length [m]
l_d diffusion length [m]
M mass [kg]
N number of full or empty states
n integer
T temperature [K]
t time [s]
V volume [m^3].

Greek symbols

β radiative relaxation quantum confined to ground state rate [s^{-1}]
δ optical penetration, or skin, depth [m]
γ radiative relaxation rate for surface to ground state [s^{-1}]
λ wavelength [m]
ν frequency [s^{-1}]
ρ density [kg m^{-3}]
σ absorption/emission cross-section [m^2]
τ characteristic decay time [s].

Subscripts

ag aged
ec excited state
fr fresh
g gap
g ground state
L,l laser
n integer n
o initial
q quantum confined state
q_a available empty quantum confined states
s surface state
st stimulated emission
T transmitted
tot total.

1. Introduction

Silicon is the dominant material in microelectronics. It is inexpensive, has versatile semiconducting properties

* Corresponding author. Current address: Seagate Technology, 7801 Computer Avenue South, Bloomington, MN 55435, U.S.A.

0017–9310/98 $19.00
PII: S0017–9310(98)00181–1

that are easily changed by doping, and most importantly, has a 'native oxide', silicon dioxide, that is easily grown to form insulating layers on silicon with extremely small surface state densities. Additionally, silicon processing technology is highly developed. Silicon has been regarded as a material unsuitable for optical applications, however, because it has an indirect band gap, making emission of light very inefficient. It also has a relatively small band gap ($E_g = 1.1$ eV), so that the light that it does emit is in the infrared portion of the spectrum, limiting its usefulness to applications requiring infrared light.

Recently, a nanostructured form of silicon, known as 'porous' silicon, has demonstrated strong visible photoluminescence at room temperature [1]. It has also been shown to electroluminesce over the entire visible spectrum, although the efficiency remains low [2, 3]. These discoveries have led to a tremendous upsurge in research into porous silicon as an optoelectronic material. There is no consensus, however, on the mechanisms involved in the photo- and electroluminescence, including the recombination and transport processes. These mechanisms must be well understood before they can be exploited for actual device applications.

An example of an important application of porous silicon is in fast optical switching. An optical switch is turned on and off by a beam of light, usually a laser. The switching behavior relies on the intensity dependent optical properties of the material. Porous silicon has been shown to exhibit nonlinear optical behavior that decays on short time scales and can be used as the basis for a fast optical switch [4–7]. Design and optimization of this type of device, however, requires detailed understanding of the absorption of laser radiation by the material and subsequent energy transfer in the material on short time scales.

Porous silicon has several unique microscopic features which make its properties and transport behavior very different from its parent, bulk crystalline silicon. Particularly important are carrier confinement, surface properties and disorder. This work examines the impact of these features on short time-scale radiative energy deposition and transfer processes in porous silicon. The unique properties of porous silicon are discussed, and a five level model of radiative energy transfer is proposed. This model is then applied to picosecond differential transmission measurements made on light emitting porous silicon samples.

2. Unique optical properties of porous silicon

Light emitting porous silicon has some characteristics which make its optical properties different from bulk silicon. First, it is a highly porous structure made up of crystallites and/or columns which are a few nm (10^{-9} m) in diameter. A human hair is in the range of 30–70 microns, or 30 000–70 000 nm, so these crystallites are extremely small. Two and three-dimensional quantum confinement can occur in these small columns and crystallites, respectively, leading to enhanced optical properties. The effects of quantum confinement are shown schematically in Figs 1 and 2. In Fig. 1, the solutions to the quantum mechanical 'particle in a box' problem are shown. Because the size of the structure is on the order of the de Broglie wavelength of the electron (hole, or electron-hole pair), the carrier is confined. Rather than being allowed the travelling wave solutions which occur in a large bulk medium, the particle's wave solution must satisfy the boundary conditions (wave function amplitude and its derivative equal zero at the boundary). Only solutions whose integer multiple half wavelengths equal the characteristic length ($n\lambda/2 = L$) satisfy this condition. This means that only discrete energy levels which correspond to these solutions are allowed and other states are forbidden. Figure 2 shows the difference between a bulk semiconductor and a quantum confined semi-

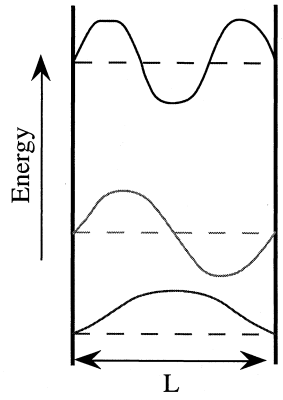

Fig. 1. Allowed solutions of the quantum mechanical 'particle in a box' problem.

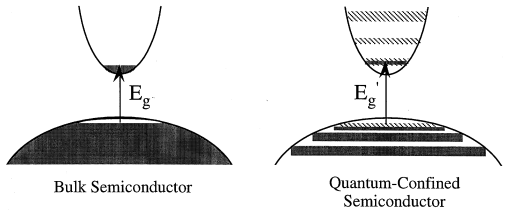

Fig. 2. Differences between a bulk semiconductor and a quantum confined semiconductor.

conductor.† Rather than all states in the conduction band being available for an excited electron, only fairly discrete energy levels are allowed.

The discrete energy levels have several effects on optical properties. First, there is an effective increase in the band gap since the minimum of the conduction band is effectively moved to the first discrete energy level. This would mean that absorption of photons by the material would be shifted to only photons of energy $E > E_g'$, greater than the effective band gap. It also means that photons emitted during radiative electron-hole recombination will be of higher energy, since they will be at the effective band-gap energy. For porous silicon this means that light may be emitted in the visible rather than the infrared portion of the spectrum, making it much more useful in optical applications.

Second, the discrete nature of the energy levels can lead to nonlinearities in optical properties. Since the state is discrete, only a finite number of electrons (holes) can be promoted to this state by absorption of a photon. When this state is full, no further photons can be absorbed. Thus, the absorption coefficient is reduced until the electrons (holes) can relax back to the ground state. This behavior can be used as the basis for an optical switch, as shown in Fig. 3. When light of sufficient intensity to fill the first energy level is incident on the material, the material can no longer absorb photons and it will transmit an optical signal—it is 'on'. When the high intensity light is not incident on the material it can continue to absorb photons and an optical signal will not be transmitted—it is 'off'. This concept has been demonstrated by Matsumoto et al. [4–6].

Finally, light emission in an indirect semiconductor like silicon can be enhanced because of quantum confinement. Normally, in an indirect band-gap semiconductor like silicon, radiative recombination requires the assistance of an extra particle (usually a phonon) for conservation of momentum since the electrons at the minimum of the conduction band are at a different point in momentum space than holes at the maximum of the valence band. This three-particle process then becomes much less likely than other, usually nonradiative, processes. In a quantum confined semiconductor, however, confinement of the electrons, holes and phonons means that their location in real space is well defined. Quantum mechanics dictates that either momentum or location can be well defined at one time, but not both. This means that the momentum of these particles is not well defined—they are spread out in momentum space—and therefore the selection rules that conserve momentum in the recombination process are relaxed. Radiative electron-hole recombination then becomes more probable.

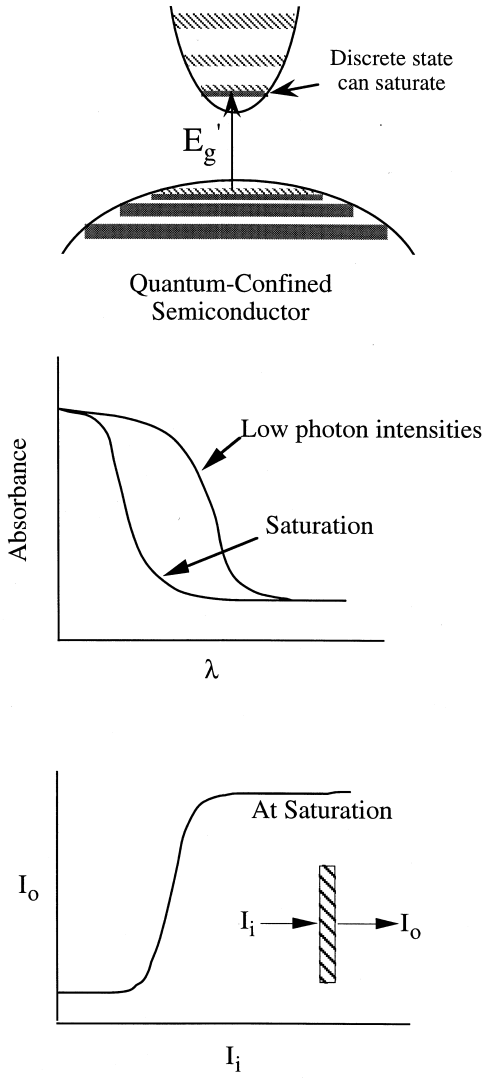

Fig. 3. Principle of discrete state saturation as basis for an optical switch.

Another important feature of porous silicon that enhances its light emitting properties is that its surface is passivated by hydrogen. This means that bonds on the silicon surface which have no silicon atom attached have a hydrogen atom attached rather than being a 'dangling bond'. Dangling bonds act as traps, or energy levels in the gap of silicon, which are delocalized in momentum

† Note that figure compares direct-gap semiconductors. The porous silicon band structure would have the additional complication of an indirect gap in which the minimum of the conduction band the maximum of the valence band are not at the same point in momentum space.

space and provide excellent nonradiative recombination centers for electrons and holes. As mentioned above, the transition rates for nonradiative recombination via traps is often faster than the radiative recombination rate in indirect-gap semiconductors. The attachment of the hydrogen atom removes the dangling bond and therefore removes the nonradiative recombination center. The reduction of nonradiative recombination centers decreases the corresponding nonradiative transition rate and therefore can increase the incidence of radiative recombination. The effect of hydrogen surface passivation is significant. Light emitting porous silicon which has been heated so that the hydrogen desorbs from the surface ceases to emit light efficiently [8]. It does not seem, however, that the surface must be passivated with hydrogen. Samples that have undergone rapid thermal oxidation and contain no hydrogen, but have a surface well passivated with oxygen atoms, usually in the form of a silicon dioxide layer, also have been shown to exhibit efficient luminescence [9].

Another feature of porous silicon that cannot be ignored is its incredibly large internal surface area and high surface-to-volume ratio. Internal surface areas of several hundred square meters per cubic centimeter are typical! [10]. In addition, as the column and crystallite size become smaller, the surface-to-volume ratio increases. Not only are there significantly more surface states than in the bulk material, but their ratio to bulk crystalline states is even higher. For example in a crystallite of 3 nm, there are 5 unit cells and about 1000 atoms total. Of these atoms, 300 are surface atoms! This means that surface states or localized states at the silicon/silicon dioxide surface are likely to play a much more important role in porous silicon than in bulk crystalline material.

Finally, the impact of disorder must not be ignored. Since the crystallites retain the crystalline nature of the original bulk silicon wafer, porous silicon is a material that still has short range order in the core of the crystallite. On the surface, however, the material must satisfy local chemistry. The bond lengths and angles will have to adjust accordingly. The relaxed surface will have Si–Si configurations much like amorphous silicon [11]. It is expected that some of these states will have energies less than the band-gap energy of the core, creating states in the gap much like the tail states in amorphous silicon. In addition, it is likely that the electron wave functions of these states will be localized due to the perturbed silicon crystallite surface. Long range order is also not preserved in porous silicon. The crystallites, particularly in the p-type material, are randomly arranged with respect to each other. In fact, small angle X-ray scattering has confirmed the fractal nature of the material [12]. The fractal nature of the structure can add its own interesting features to the optical properties through the introduction of additional vibrational modes that are related to the fractal structure [13].

3. Short time-scale optical properties

Radiative and nonradiative transitions in porous silicon occur on time scales from fs to ms. At long times and/or steady state, many of these processes occur essentially instantaneously and so there are always carriers in the ground state to absorb photons and the absorption of photons by carriers in the excited states is comparatively negligible. In short time-scale applications, however, the energy states of carriers and their short time-scale transitions between these states become important. The transient carrier dynamics lead to changes in optical properties which affect the energy absorption in the material. In ultrashort-pulse, high intensity laser-material interactions, for example, carriers may be in excited states during most of the pulse duration.

A five level system for the hybrid quantum confinement-surface state model is proposed and shown in Fig. 4. This is an expansion of the three level system proposed by Matsumoto et al. [5, 6]. which takes into consideration excited state absorption. Initially, the carriers are in the ground state (electrons in the valence band). Absorption of a photon creates an electron-hole pair that is promoted to the excited state of the quantum-confined nanocrystal. The carrier quickly relaxes nonradiatively to the lowest level of the quantum confined state on the fs time scale. From this point the carrier can relax out of the quantum confined state by direct radiative or nonradiative recombination to the ground state or by nonradiative relaxation to the surface localized state. From ps photoluminescence (PL) decay data [14] that shows a weak, blue PL band with an exponential ns decay and a strong, red-orange PL band with a nonexponential decay, it can be determined that the direct radiative transition has a ns relaxation time and the nonradiative transition to the surface state has tens of ps relaxation time.

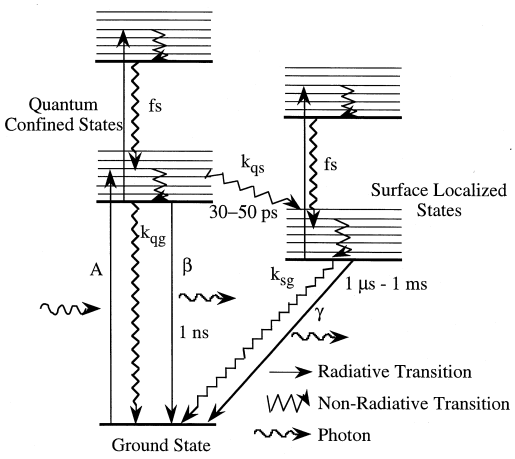

Fig. 4. Five level model of radiative and nonradiative transitions in porous silicon.

In addition, nonradiative recombination via dangling-bond traps is significantly reduced because of hydrogen passivation of the surface and the mobility reduction due to confinement. This results in most of the carriers relaxing to the surface state, but some making the direct radiative or nonradiative transition. Once in the surface state, the carriers can recombine radiatively or non-radiatively to return to the ground state with the range of μs to ms relaxation times. Rate equations valid for ps time scales can then be derived for the three primary levels

$$\frac{dN_q}{dt} = -(\beta + k_{q-g} + k_{q-s})N_q + (A_{g-q}N_gN_{q_a} - \sigma_{st}N_q)\frac{I}{h\nu} \quad (1)$$

$$\frac{dN_s}{dt} = k_{q-s}N_q - (\gamma + k_{s-g})N_s \quad (2)$$

$$\frac{dN_g}{dt} = (\sigma_{st}N_q - A_{g-q}N_gN_{q_a})\frac{I}{h\nu} + (\beta + k_{q-g})N_q + (\gamma + k_{s-g})N_s \quad (3)$$

$$N_{tot} = N_g + N_q + N_s \quad (4)$$

$$N_{q_a} = N_{q_{tot}} - N_q \quad (5)$$

β and γ are the transition rates for the radiative transitions. The transition rates for the nonradiative transitions are denoted by k. σ_{st} is the stimulated emission cross section. N is the number of carriers in the ground, quantum confined and surface states. Most of the transitions in this situation only change due to the time dependence of the number of carriers in the initial state. As discussed below, however, the fundamental absorption process, coefficient A_{g-q}, is dependent on both the number of carriers in the ground state and the finite number of empty states available in the discrete quantum confined state. N_{q_a} refers to the number of empty states available in the discrete quantum confined level and equation (5) quantifies the finite number of these available states. Equations are not written for the upper quantum confined and surface states because it is assumed that the transition out of these states occurs on a faster time scale than is considered here. In other words, the carrier will be excited and return to the lower level almost instantaneously. Once the key parameters in these equations are determined experimentally, these equations can be solved and used to predict the transient optical properties for short time-scale applications.

The primary absorption process is the ground-to-quantum confined state transition—essentially the band to band electron-hole pair creation process. This process is dependent on the number of carriers in the ground state and how many empty states are available in the quantum confined state

$$\alpha_{g-q}(t) \propto N_g(t) \cdot N_{q_a}(t), \quad (6)$$

where $\alpha_{g-q}(t)$ is the time dependent absorption coefficient for the fundamental ground-to-quantum confined state transition, $N_g(t)$ is the number of carriers in the ground state, and $N_{q_a}(t)$ is the number of empty states available in the quantum confined state. Note that since the quantum confined state is a discrete energy level, there is a finite number of available empty states. Under high intensity, short-pulse laser irradiation, this state can become filled, or saturated. At this point, no further photons can be absorbed by promotion of a carrier in the ground state to the quantum confined state, and the absorption decreases accordingly. This process is known as *bleaching*.

Photons can also be absorbed by promotion of the already photo-excited carriers in the quantum confined states or localized surface states to a higher energy level, if available. This process is known as photoinduced *absorption*. In a bulk semiconductor, absorption by the excited carriers is known as free carrier absorption and involves intraband transitions. In a high quality, undoped crystalline semiconductor very few of these transitions occur because of k-vector (momentum) conservation rules which require interaction with a phonon or impurity. As a result, photoinduced absorption is usually small in pure, crystalline materials. Intraband transitions become more likely in the presence of disorder, however, because of increased electron-lattice scattering processes as well as the smearing of the k-vector of spatially localized states. For example, photoinduced absorption is observed in amorphous silicon [15]. For the discrete states, there is not a full band of allowed states, so the photon energy must correspond with a transition to one of the higher discrete energy levels for excited state absorption to occur. The localized surface states can also be involved in the photon absorption process and have the advantage mentioned above of spatial localization leading to relaxation of k-vector selection rules.

Excited carrier absorption would then similarly be related to the number of carriers in the lower excited state and the number of empty carriers in the upper excited state. Nonradiative relaxation from the upper excited state usually occurs on fs time scales, so it is reasonable to assume that the upper excited states are empty and that the carriers that are excited to the upper state relax very quickly again to the lower state. Thus, the only time dependency in the excited state absorption is the number of excited carriers

$$\alpha_{ec}(t) = \sigma_q N_q(t) + \sigma_s N_s(t), \quad (7)$$

where α_{ec} is the excited state absorption coefficient, N_q and N_s are the number of carriers in the quantum confined and surface localized states, respectively, and σ_q and σ_s are the absorption cross sections of the quantum confined and surface localized state, respectively. The total absorption coefficient is then

$$\alpha(t) = A_{g-q}N_g(t)N_{q_a}(t) + \sigma_q N_q(t) + \sigma_s N_s(t). \quad (8)$$

Whether bleaching or photoinduced absorption is

observed depends on several factors. First, it depends on the absorption cross section of the excited states. If these cross sections are on the order of that of the ground state, then photo-induced absorption will be a significant transient effect. As discussed above, the excited state absorption cross section is low in pure, crystalline materials and higher in disordered materials. Bleaching can be a dominant effect if the excited state absorption is fairly low and the states are easily saturated. Because of the finite number of states in the discrete energy levels of a quantum confined semiconductor, bleaching is usually observed. In porous silicon, however, there is a wide distribution of sizes of nanocrystals, which can lead to a wide distribution of 'discrete' energy levels. Because of this, discrete absorption, observed in other discrete systems like molecules and quantum dots of narrow size distribution, has not been observed. This wide size distribution may also impact the bleaching of the quantum confined states. If a variety of sizes leads to a spread of energy levels available for photon absorption, then no one discrete state may become saturated. If, however, discrete bleaching levels are observed, it is strong evidence of the quantum confinement.

4. Differential transmission measurements

There have been several studies looking at the short time-scale behavior of porous silicon, but the results have been varied and somewhat conflicting. In addition, little attention was paid to the fresh or aged condition of the porous silicon. Hipwell et al. [16], therefore, performed ps differential transmission experiments aimed at clarifying the short time-scale dynamics. Particular attention was paid to the aged condition of the samples. Further details of the experiments can be found in [16]. The model derived in the last section can be applied to these results, providing an improved understanding of short time-scale carrier dynamics in porous silicon.

Picosecond pump-probe differential transmission spectra are shown in Figs 5 and 6 for various times. Because the zero will not be the same for all wavelengths due to chirp, zero is not set at the peak response. Zero time is merely the first data point. The response of the sample in time can more clearly be seen in Figs 7 and 8. These figures show the differential transmission change integrated over a 12 nm wavelength section. Multiple wavelength ranges are shown on each graph.

There are several notable observations to be made about the differential transmission spectra. First, it is seen that in both types of samples a negative signal—induced absorption—is observed. No bleaching is observed at any wavelength. Second, the induced absorption change is much stronger in the fresh, nonluminescing sample than in the aged, highly luminescent sample. Third, there seem to be two components: a fast, wavelength dependent component and a slower relaxing component that has no wavelength dependence. As can be seen clearly in Fig. 5, after 333.5 ps there is still a negative 2% transmission change that has no wavelength dependence. There is a strong wavelength dependent part of the signal, however, that reaches a peak at the 133.4 ps point (near the zero point) and has almost completely disappeared by 333.5 ps. Both these components seem to be present in the aged sample as well, though it is not as pronounced.

An estimate for decay times is first made by fitting single and double exponential decays to the integral transmission changes. Good estimates will be obtained in this way if the decay time is significantly larger than the pulse width (usually three times larger is considered to be sufficient). The pulse can then be considered to be like an impulse. The decay times found by the exponential fitting are shown in Table 1. Most satisfy the criterion to use the exponential decay fit. The decay times noted were obtained from the slope of an apparent linear fit on a ln[− (integral differential transmission)] vs time plot (see asterisk in Table 1), whereas the others were obtained by a direct fit of an exponential decay function on the −(integral differential transmission) vs time plot. Interestingly enough, the samples in the 580–700 nm range were well fit by single exponential functions, but the fresh samples in the 680–800 nm range were difficult to fit with single exponentials and often appeared to be better fit by a double exponential with one decay time very similar to that found for the single exponentials. This result is in line with the strong two component behavior that is observed in Fig. 5, particularly since the second component appears to only be significant at wavelengths greater than 675 nm.

A picture of the short time-scale carrier dynamics and optical properties can be drawn from the above results. The carriers are first excited into the quantum confined nanocrystals, having an increased band gap due to the confinement. Due to the confinement and disorder effects on the k-vector selection rules, intraband transitions are more probable than in high quality bulk silicon and photoinduced absorption is observed. Additionally, bleaching due to discrete state filling is not observed because of the broad distribution of nanocrystal sizes. Free carrier absorption, having a wavelength dependence of λ^p, where p is 1.5–3.5 [17], near the band edge in the fresh sample explains the strong wavelength dependent contribution above 675 nm. The signal is not as strong in the aged sample because the measurements are taken at energies more significantly above the sample's band gap. The carriers relax out of this state on a hundreds of picosecond time scale into localized surface states. A large number of surface states near the Fermi level in the gap, $N(E_F \sim 10^{19}\ \mathrm{eV}^{-1}\ \mathrm{cm}^{-3}$, were found in the experiments of Ben–Chorin et al. [18], so it not surprising that absorption by these states, being localized and having relaxed k-vector selection rules, is significant. Radiative recom-

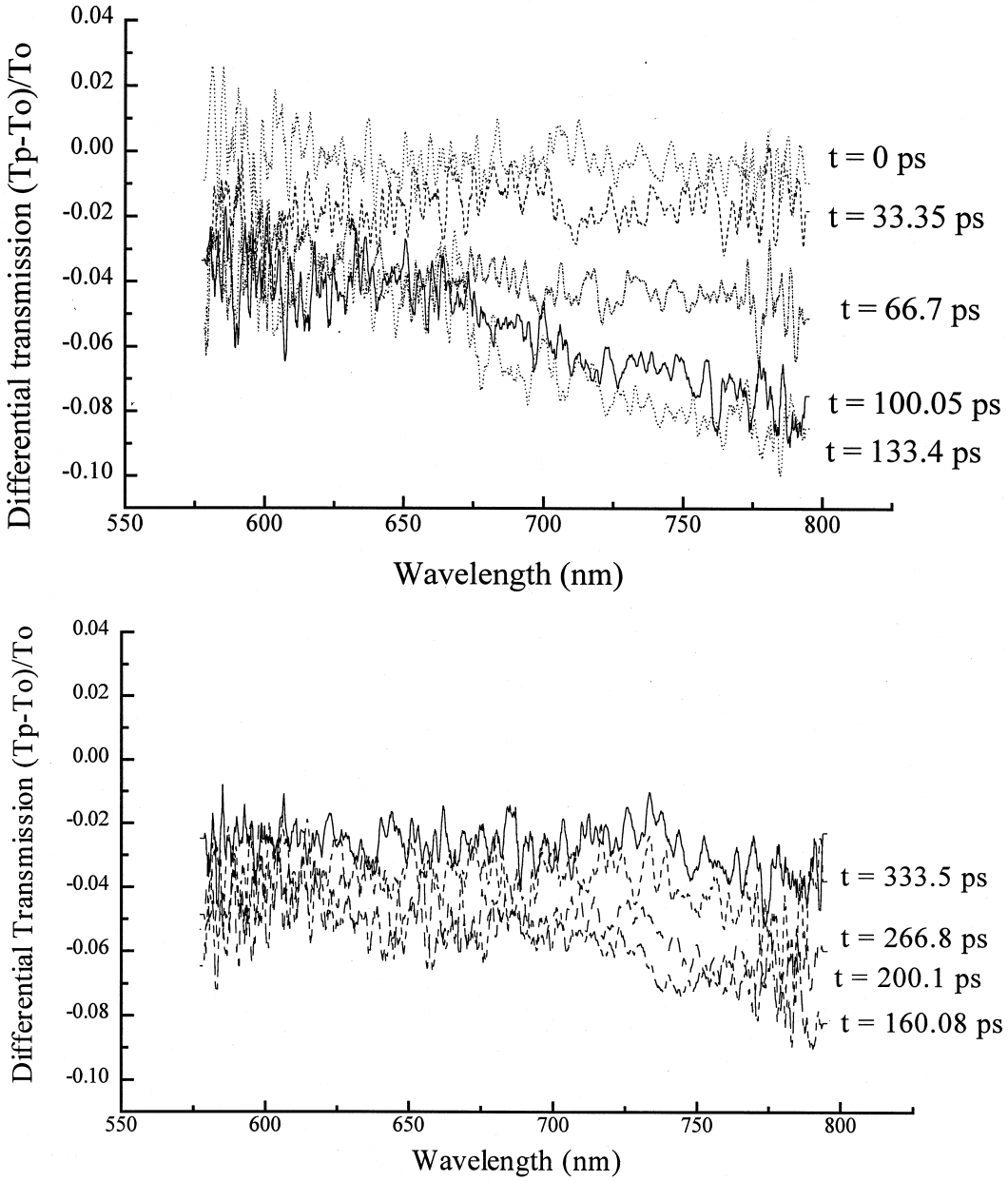

Fig. 5. Differential transmission spectra of a fresh sample at several times.

bination out of this state on the μs to ms time scale is then responsible for the steady-state, red-orange luminescence.

This picture is consistent with that proposed by Matsumoto et al. [5, 6] based upon their fs photoluminescence and nonlinear absorption measurements. It is also consistent with the recent fs results of Klimov et al. [19]. Fauchet [20] attributed the ps decay to Auger recombination. Delerue et al. [21] showed that in a confined nanocrystal the Auger recombination process was still effective and the relaxation time could be reduced to the 100 ps–100 ns range. If this process was responsible for the 100 ps decay, then a thermally induced change in band gap which would have a ms decay time could be responsible for the longer time scale-component.

Thermal effects must be considered since the optical properties of bulk silicon are highly temperature dependent [22]. This can be seen in Fig. 9, where differential

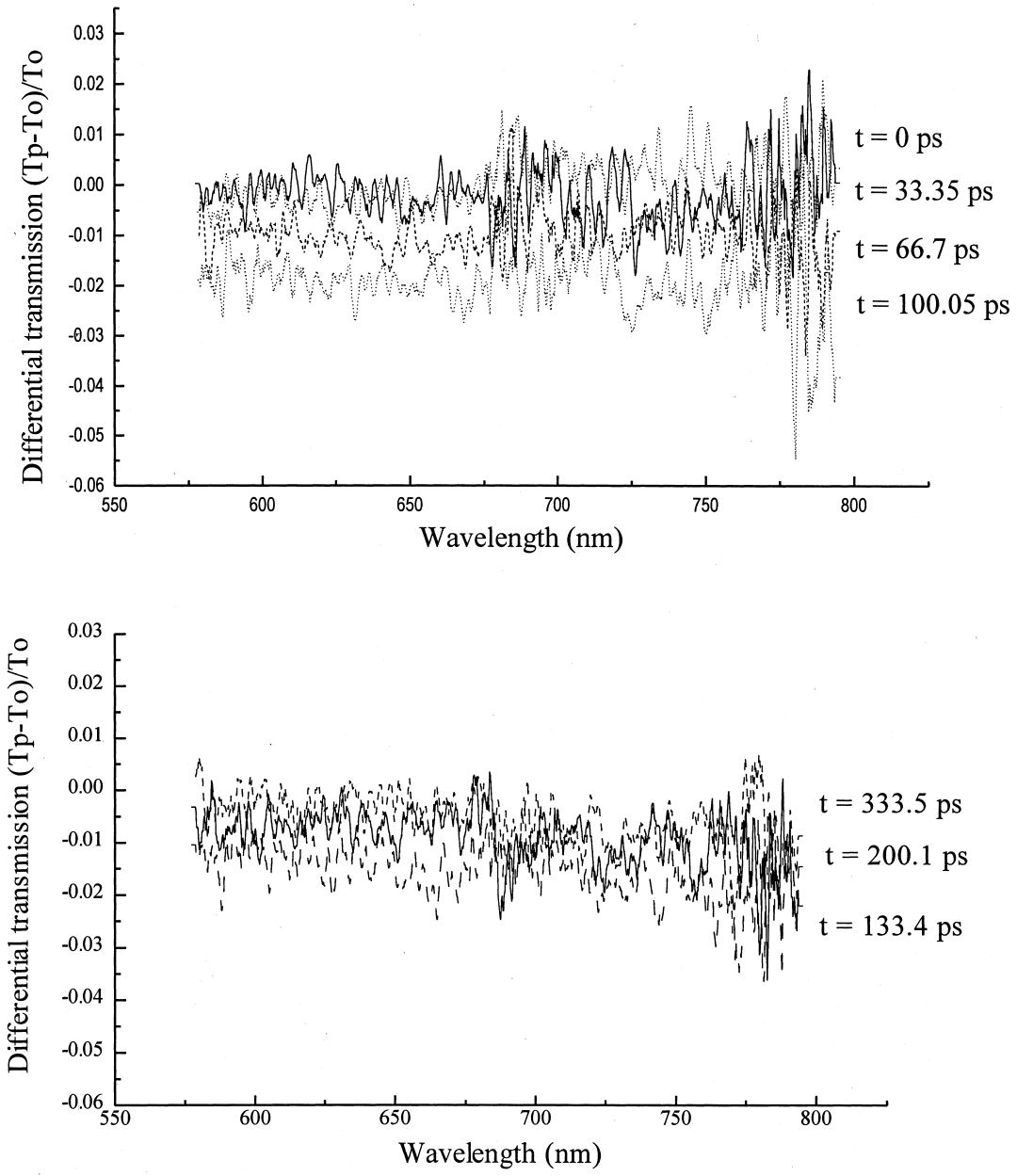

Fig. 6. Differential transmission spectra of an aged sample at several times.

transmission changes with temperature of a 1 μm film are plotted using the empirical relation and constants of Jellison and Modine [22]. A classical conduction analysis was performed for the samples used in this experiment [23]. The solution was found to be multiexponential with decay times, τ, of

$$\tau_n = \frac{4h^2}{n^2\pi^2 D_{\text{th}}}. \tag{9}$$

The first five decay times for this film are therefore 32, 8, 3.5, 2, and 1.3 μs, using $D_{\text{th}} = 1.83 \times 10^{-6}$ m^2 s^{-1} [23]. These components have decreasing contribution to the solution as it converges. The first decay time, 32 μs, therefore has the largest contribution. The Fourier number, or dimensionless time, is

$$Fo = \frac{l^2}{D_{\text{th}}} = 79\,\mu\text{s}, \tag{10}$$

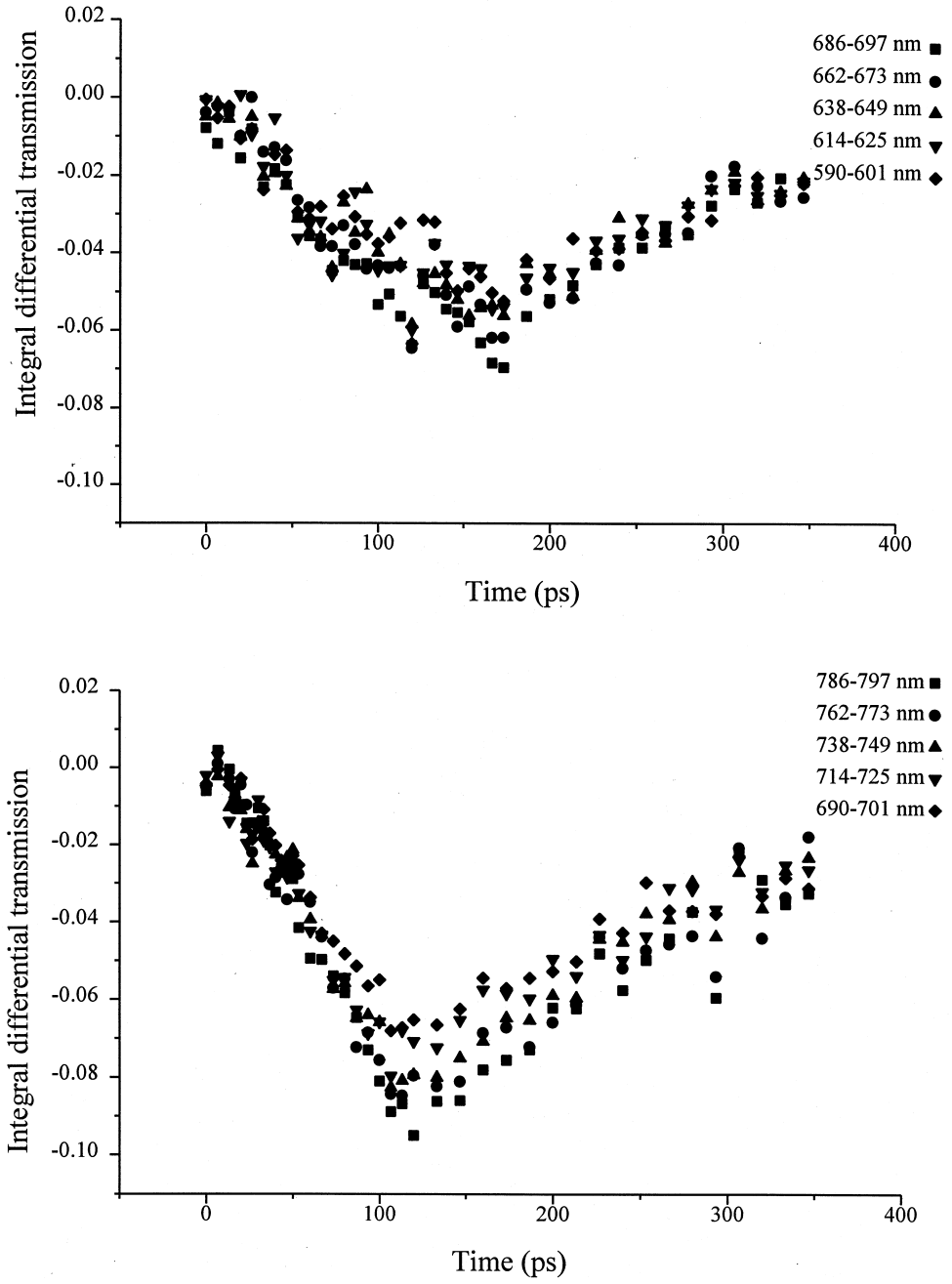

Fig. 7. Integral differential transmission vs time for several wavelength ranges, fresh sample.

where the characteristic length, l, is the film thickness, h. These decay times are close to the 100 s of μs–ms decay times observed in the experiments, so a thermal contribution is a possibility. It is important to note, however, that from this analysis, the decay time is dependent only on film thickness and thermal diffusivity of the film. Matsumoto et al. [4] observed a dependence of decay time on laser intensity, which is contrary to a thermal explanation of the long time scale component.

The other factor that must be considered is the magnitude of the differential transmission change by the heating in these experimental situations. The average tem-

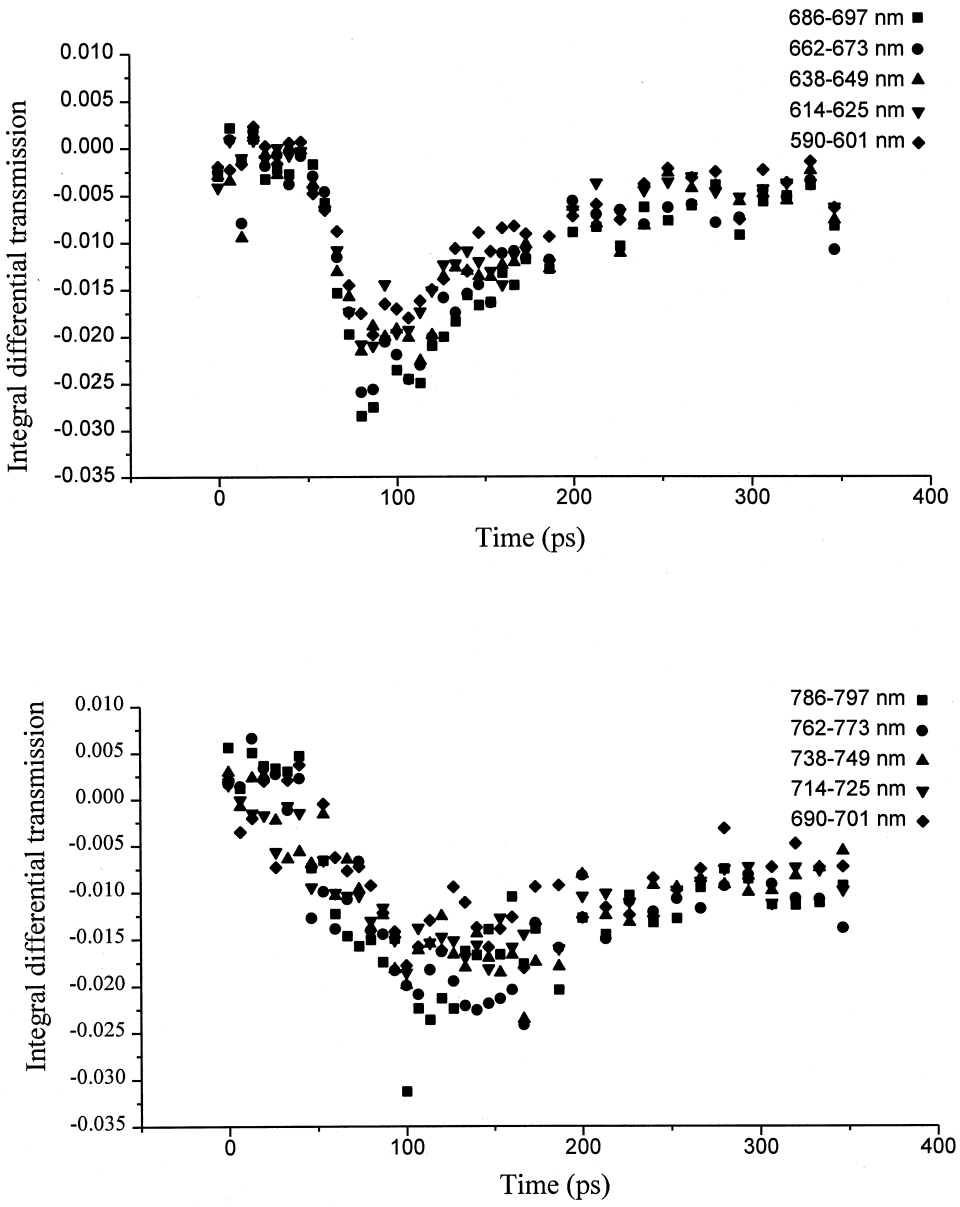

Fig. 8. Integral differential transmission vs time for several wavelength ranges, aged sample.

perature rise within an optical depth can be used to get an estimate of the change in the temperature and thus the optical properties. In the current experiment, 12 μm porous silicon films were heated by a Nd:YAG laser at 532 nm and a 2.5 mJ pulse energy. By extrapolation of the apparently linear decrease in transmission [16], the optical properties at 532 nm can be obtained. The percent transmission for the fresh sample would be 30% and that of the aged sample would be 18%. Since $I_T/I_o = e^{-\alpha x}$, the corresponding absorption coefficients and penetration depths are then $\alpha_{fr} = 1000$ cm^{-1}, $\delta = 10$ μm and $\alpha_{ag} = 1430$ cm^{-1}, $\delta = 7$ μm. The maximum average temperature rise in the film is

$$\Delta T = \frac{E_L}{V\rho C_p}, \tag{11}$$

where E_L is the laser energy, V is the absorption volume (beam spot size $\times$ absorption depth), ρ is the density, and C_p is the specific heat. The density is multiplied by 1-porosity and the specific heat of bulk silicon is used.

Table 1
Decay times of the negative integral differential transmission signal for each wavelength range

Wavelength range	Decay time (ps)	
	Fresh	Aged
578–589	102.8	98
590–601	113.5	127.2
602–613	148.0	80
614–625	79.3	138
626–637	182.5	120
638–649	73.2	128.4
650–661	118.7	120.5
662–673	129.6	116
674–685	205.8*	96
686–697	193.8*	116
678–689	187.6*	67.15
690–701	190.1*	780
702–713	181.8*	158.14
714–725	170.1*	190*
726–737	180.8*	246.3*
738–749	175.1*	263.85
750–761	200.8*	374.8
762–773	204.92*	222.6
774–785	242.1*	244.5*
786–797	263.9*	228.8*

* See text for explanation.

Using equation (11), $\Delta T_{fr} = 13.5$ K and $\Delta T_{ag} = 19.3$ K. Assuming the same temperature dependence of absorption coefficient as bulk silicon, this corresponds to 3.2 and 4.6% increase in absorption coefficient, respectively. The corresponding differential transmission changes would be 0.034 and 0.077, respectively. These are higher than the longer time component in the experiments. This fact is not necessarily an issue, because the temperature dependence of bulk silicon was used and the temperature dependence of porous silicon is not known. Additionally, the signal for the aged sample is stronger, which is contradictory to the experimental observations. Unless there is some reason for the aged sample to have less temperature dependence in optical properties than the fresh sample, this qualitative observation does not support a thermal origin to the long time-scale component.

There are several facts that support a non-thermal origin to the longer time-scale component. The lack of spectral dependence in differential transmission is one of them. A definite spectral dependence for differential transmission was observed in Fig. 9 for bulk silicon. In addition, Matsumoto et al. [4] observed an intensity dependent change in decay time for the longer time-scale component. As shown in equations (9) and (10), the thermal decay time depends only on material properties and film thickness. Finally, the decay time seems to correspond very well to the observed decay time of the red-orange photoluminescence band in porous silicon. If most radiative and nonradiative decay happens on the ms time scale, then heating will happen on this time scale as well. These observations support the surface state recombination mechanism.

The data are contradictory with the ps measurements made under very similar conditions by Klimov et al. [7] which have not been reproduced by any other group. They observed very strong bleaching of discrete states similar to that obtained in quantum confined nanocrystals of CdS and CdSe. They attributed this to saturation of a certain size of discrete state in quantum confined nanocrystals of silicon. The difference in their experiment was that the porous silicon samples were fabricated from n^+-type substrates and therefore would be made up of quantum wire rather than quantum dot type structures. Their explanation for later photoinduced absorption results on similar samples [19] was that the pump energy for the later experiment was different and would have resonantly excited a different component (molecular-like clusters) in the porous silicon. The current experiments, however, use the same pump energy as the original experiments, 532 nm, yet no discrete bleaching is observed—even in brightly luminescent samples which would be expected to have quantum confined nanocrystals. The only difference which can reasonably explain this discrepancy would be if there is a narrower distribution of quantum wire diameters in n^+-type porous silicon than the distribution of quantum dot diameters in p^--type porous silicon. To date, this observation has not been made. Additionally, it is difficult to believe that no nanocrystal size existed in the p^- porous silicon which would have a resonant interaction with the 2.33 eV (532 nm) pump energy.

A final note is that the ps or several ps component observed in the fs measurements of Fauchet [20], Klimov et al. [19], and Matsumoto et al. [5, 6] was not observable in these measurements due to the ps time resolution. This component is often attributed to carrier thermalization in the nanocrystal, however, which is not inconsistent with the above picture of carrier dynamics.

5. Conclusions

Porous silicon has the unique characteristics of confinement, high surface area, and disorder on several length scales, which cause it to possess enhanced optical properties. Short time-scale properties and radiative transfer are examined in this work. A five level system is presented to model the carrier dynamics among the ground, quantum confined and localized surface states. Bleaching, or absorption saturation, is predicted to be important for the discrete quantum confined states of porous silicon if the size distribution is small enough to

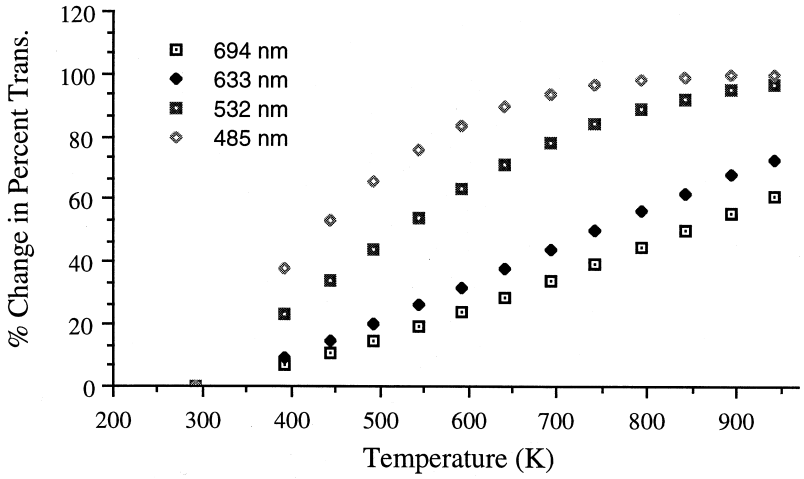

Fig. 9. Percent change in percent transmission relative to room temperature vs temperature for a 1 μm film of bulk silicon selected laser wavelengths.

create narrow bands to be filled. Photoinduced absorption is shown to be important in semiconductors with a high degree of disorder because of the increased occurrence of scattering events and k-vector rule relaxation.

The model is applied to picosecond differential transmission measurements on porous silicon. These measurements exhibited photoinduced absorption in all samples with both broad band and wavelength dependent components. The integral absorption shows 100–200 ps exponential decay. This is consistent with the proposed model based upon initial optical excitation into quantum confined nanocrystals with a broad distribution of sizes and subsequent relaxation into localized surface states on a hundreds-of-ps time scale. Free carrier absorption is enhanced by the disorder and confinement. The localized surface states are then proposed to be the source of the steady-state, red-orange luminescence. The results are additionally discussed in light of the results of other short time-scale studies.

Acknowledgements

Support from the National Science Foundation and the Department of Energy is gratefully acknowledged.

References

[1] L.T. Canham, Silicon quantum wire array fabrication by electrochemical and chemical dissolution of wafers, Appl. Phys. Lett. 57 (1990) 1046–1048.

[2] A. Halimaoui, C. Oules, G. Bomchil, A. Bsiesy, F. Gaspard, R. Herino, M. Ligeon, F. Muller, Electroluminescence in the visible range during anodic oxidation of porous silicon films, Appl. Phys. Lett. 59 (1991) 304–306.

[3] A. Bsiesy, F. Muller, M. Ligeon, F. Gaspard, R. Herino, R. Romestain, J.C. Vial, Relation between porous silicon photoluminescence and its voltage-tunable electroluminescence, Appl. Phys. Lett. 65 (1994) 3371–3373.

[4] T. Matsumoto, M. Daimon, H. Mimura, Y. Kanemitsu, N. Koshida, Optically induced absorption in porous silicon and its application to logic gates, J. Electrochem. Soc. 142 (1995) 3528–3533.

[5] T. Matusomoto, T. Futagi, H. Mimura, Y. Kanemitsu, Ultrafast decay dynamics of luminescence in porous silicon, Phys. Rev. B. 47 (1993) 13876–13879.

[6] T. Matsumoto, O.B. Wright, T. Futagi, H. Mimura, Y. Kanemitsu, Ultrafast electronic relaxation processes in porous silicon, J. Non-Cryst. Solids 164–166 (1993) 953–956.

[7] V.I. Klimov, V.S. Dneprovskii, V.A. Karavanskii, Nonlinear-transmission spectra of porous silicon: manifestation of size quantization, Appl. Phys. Lett. 64 (1994) 2691–2693.

[8] E. Bassous, M. Freeman, J.-M. Halbout, S.S. Iyer, V.P. Kesan, P. Munguia, S.F. Pesarcik, B.L. Williams, Characterization of microporous silicon, fabricated by immersion scanning, Mat. Res. Soc. Symp. Proc. 256 (1992) 23–26.

[9] V. Petrova-Koch, T. Muschik, A. Kux, B.K. Meyer, F. Koch, V. Lehmann, Rapid-thermal oxidized porous Si—the superior photoluminescent Si, Appl. Phys. Lett. 61 (1992) 943–945.

[10] B. Hamilton, Porous silicon, Semicond. Sci. Technol. 10 (1995) 1187–1207.

[11] F. Koch, Models mechanisms for the luminescence of porous Si, Mat. Res. Soc. Symp. Proc. 298 (1993) 319–329.

[12] P. Goudeau, A. Naudon, G. Bomchil, R. Herino, X-ray small-angle scattering analysis of porous silicon layers, J. Appl. Phys. 66 (1989) 625–628.

[13] V.A. Markel, E.B. Stechel, W. Kim, R. Armstrong, V. Shalaev, Optical properties of fractal nanocomposites, Mat. Res. Soc. Symp. Proc. 367 (1995) 417–422.

[14] F. Koch, V. Petrova-Koch, T. Muschik, A. Nikolov, V. Gavrilenko, Some perspectives on the luminescence mechanism via surface-confined states of porous Si, Mat. Res. Soc. Symp. Proc. 283 (1992) 197–202.
[15] Z. Vardeny, J. Tauc, Picosecond electronic relaxation in amorphous semiconductors, in: R.R. Alfano (Ed.), Semiconductors probed by ultrafast laser spectroscopy, Vol. II, Academic Press, 1984, 25–53.
[16] M.C. Hipwell, C.L. Tien, X.L. Mao, R.E. Russo, Picosecond differential transmission measurements on porous silicon, Microscale Thermophys. Eng. 2 (1998) 87–89.
[17] J.I. Pankove, Optical Processes in Semiconductors, Dover Publications, New York, 1971.
[18] M. Ben-Chorin, F. Moller, F. Koch, W. Schirmacher, M. Eberhard, Hopping transport on a fractal: ac conductivity of porous silicon, Phys. Rev. B. 51 (1995) 2199–2213.
[19] V. Klimov, D. McBranch, V. Karavanskii, Strong optical nonlinearities in porous silicon: femtosecond nonlinear transmission study, Phys. Rev. B. 52 (1995) R16989–R16992.
[20] P.M. Fauchet, Ultrafast carrier dynamics in porous silicon, Phys. Stat. Sol. B. 190 (1995) 53–62.
[21] C. Delerue, M. Lannoo, G. Allan, E. Martin, I. Mihalcescu, J.C. Vial, R. Romestain, F. Muller, A. Bsiesy, Auger and Coulomb charging effects in semiconductor nanocrystallites, Phys. Rev. Lett. 75 (1995) 2228–2231.
[22] G.E. Jellison Jr., F.A. Modine, Optical absorption of silicon between 1.6 and 4.7 eV at elevated temperatures, Appl. Phys. Lett. 41 (1982) 180–182.
[23] M.C. Hipwell, Short time-scale energy transport in light-emitting porous silicon, Ph.D. thesis, University of California, Berkeley, CA, 1996.